



1 **Surface formation, preservation, and history of low-porosity crusts at the**
2 **WAIS Divide site, West Antarctica.**

3 John M. Fegyveresi^{1,2}, Richard B. Alley², Atsuhiko Muto³, Anaïs J. Orsi⁴,
4 Matthew K. Spencer⁵

5
6 ¹Terrestrial and Cryospheric Sciences Branch, U.S. Cold Regions Research and
7 Engineering Laboratory (CRREL), Hanover, NH, 03755, USA.

8
9 ²Dept. of Geosciences, and Earth and Environmental Systems Institute, Pennsylvania
10 State University, University Park, PA, 16802, USA.

11
12 ³Dept. of Earth and Environmental Science, College of Science and Technology, Temple
13 University, Philadelphia, PA, 19122, USA.

14
15 ⁴Laboratoire des Sciences du Climat et de l'Environnement, LSCE/IPSL, CEA-CNRS-
16 UVSQ, Université Paris-Saclay, F-91191, Gif-sur-Yvette, France.

17
18 ⁵School of Physical Sciences, Lake Superior State University, Sault Sainte Marie, MI,
19 49783, USA.

20

21

22 *Correspondence to:*

23 J. M. Fegyveresi (fegy.john@gmail.com; john.m.fegyveresi@usace.army.mil)

24 **Key Words:**

- 25 • Antarctic snow surface, ice cores, field observations, snow-surface crusts, bubble-
26 free layers, vapor transport, firn properties, snow physics.

27

28

29

30

31



32

Abstract

33 Observations at the WAIS Divide site show that near-surface snow is strongly altered by
34 weather-related processes such as strong winds and temperature fluctuations, producing features
35 that are recognizable in the deep ice core. Prominent “glazed” surface crusts develop frequently at
36 the site during summer seasons. Surface, snow pit, and ice core observations made in this study
37 during summer field seasons from 2008-09 to 2012-13, supplemented by Automated Weather
38 Station (AWS) data with insolation sensors, revealed that such crusts formed during relatively
39 low-wind, low-humidity, clear-sky periods with intense daytime sunshine. After formation, such
40 glazed surfaces typically developed cracks in a polygonal pattern with few-meter spacing, likely
41 from thermal contraction at night. Cracking was commonest when several clear days occurred in
42 succession, and was generally followed by surface hoar growth; vapor escaping through the
43 cracks during sunny days may have contributed to the high humidity that favored nighttime
44 formation of surface hoar. Temperature and radiation observations showed that daytime solar
45 heating often warmed the near-surface snow above the air temperature, contributing to mass
46 transfer favoring crust formation and then surface hoar formation. Subsequent investigation of the
47 WDC06A deep ice core revealed that crusts are preserved through the bubbly ice, and some occur
48 in snow accumulated during winters, although not as commonly as in summertime deposits.
49 Although no one has been on site to observe crust formation during winter, it may be favored by
50 greater wintertime wind-packing from stronger peak winds, high temperatures and steep
51 temperature gradients from rapid midwinter warmings reaching as high as -15°C , and perhaps
52 longer intervals of surface stability. Time-variations in crust occurrence in the core may provide
53 paleoclimatic information, although additional studies are required. Discontinuity and cracking
54 of crusts likely explain why crusts do not produce significant anomalies in other paleoclimatic
55 records.



56 **1: Introduction**

57 Visual and thin-section examination of the WAIS Divide deep ice core from West
58 Antarctica revealed an annual signal linked to bubble and grain characteristics [Fitzpatrick et al.,
59 2014], but also numerous crusts. These crusts are bubble-free or nearly so, typically one grain and
60 1 mm or less in thickness, and are readily identified visually in bubbly ice (Fig. 1). Their presence
61 in greater abundance than seen in most cores [e.g., Alley, 1988] motivated studies to understand
62 their formation, possible influence on other paleoclimatic data, and potential for recording
63 paleoclimatic conditions themselves.

64 Work by Orsi et al. [2015] and Mitchell et al. [2015] showed that no significant artifacts
65 are introduced to paleoclimatic records by the WAIS Divide crusts. Here, we report additional
66 studies showing that summertime crusts form under specific conditions linked to persistent high-
67 pressure systems, so the time-series of crusts likely contains paleoclimatic information; however,
68 many additional issues must be addressed before useful climate histories could be constructed
69 confidently.

70 Bubble-free layers much thicker than the bubble-free crusts discussed here are sometimes
71 observed in ice cores from warm sites, and provide evidence of refrozen meltwater [e.g., Das and
72 Alley, 2005]. These are of interest as paleoclimatic records but have the potential to anomalously
73 distort records of trapped gases or other components of ice cores. Refrozen meltwater can be
74 identified by an excess of trapped heavy noble gases, so Orsi et al. [2015] analyzed WAIS Divide
75 samples containing bubble-free crusts, finding that not enough meltwater was involved to
76 significantly perturb records of other trace gases. Additionally, crusts might greatly modify gas
77 trapping in the firn, but measured nitrogen-isotopic ratios at WAIS Divide show that gravitational
78 fractionation occurs down to the normal trapping depth where normal amounts of air are trapped,



79 demonstrating that the crusts are not both impermeable and laterally extensive at shallow depth
80 [Mitchell et al., 2015; Battle et al., 2011].

81 Here, we report coordinated observations of crust formation over five summers (2008-09
82 to 2012-13) at the WAIS Divide site, involving daily observations of surface evolution, shallow
83 snow-pit studies with a 2-m pit at least once per year, insolation measurements, and near-surface
84 temperature profiling, supplemented with data from an on-site automated weather station (AWS).
85 We find that crusts form most commonly in the summer but do also form in winter. In summer,
86 crust formation primarily results from the effects of strong diurnal temperature cycling under
87 clear-sky, low-wind, relatively warm conditions. Wintertime observations are not available, but
88 the physical understanding gained from our summertime data suggests hypotheses for formation.
89 Time-trends in the occurrence of summertime crusts in the core may reveal changes in the
90 frequency of the persistent high-pressure conditions that generate crusts, although additional work
91 will be required to quantify this.

92 **2: Methods**

93 The main methods used are described here. Additional details are provided in Fegyveresi
94 [2015]. The surface was observed continually by one of us (JF) during the five field seasons
95 extending from 2008-09 to 2012-13 (Table 1). During each austral summer, a back-lit snow pit
96 was also prepared and studied. All pits were sited within 1 km radius of the primary ice-core
97 drilling facility, but avoided regions disturbed by camp operations or the “drift tail” of enhanced
98 accumulation downwind of the camp. Following prior practice [e.g., Benson, 1962; Koerner,
99 1971; Alley, 1988], each sampling site involved excavating a pair of ~2 m cubic pits separated by
100 a wall ~0.5 m thick, with one pit left open to supply back-light, and the other a roofed observation
101 pit. Features such as crusts and hoar layers were easily identifiable from the observation pit on the



102 back-lit wall (Fig. 2). Pit walls were observed, mapped, sampled, and photographed (tripod-
103 mounted $> \frac{1}{4}$ s exposures). Each pit was oriented so the prevailing wind direction, approximately
104 north-south, ran from right-to-left along the back-lit wall.

105 An automatic weather station (AWS) on site at WAIS Divide (named Kominko-Slade in
106 the University of Wisconsin AWS system; Lazzara et al. [2012]), collected data on temperature,
107 air pressure, wind, and humidity starting in the 2009-10 season (all dates and times are GMT).
108 Beginning in 2011-12, upward-facing and downward-facing short-wave Li-Cor LI200
109 pyranometers were added initially 1 m above the surface to measure incoming and outgoing
110 shortwave radiation (0.4-1.1 μm spectral response). Both sensors were newly calibrated and
111 mounted in a cosine-corrected head (for solar angles up to 80°), with typical operational errors in
112 daylight of $\pm 3\%$ (max $\pm 5\%$). A Kipp-Zonen CNR2 net radiometer with upward- and downward-
113 facing pyranometers and pyrgeometers was added on an AWS mounting arm during the 2012-13
114 season, in order to measure both net short- and long-wave radiation. The pyranometers operated
115 with a spectral response of 0.3 – 2.8 μm , operational errors of $\pm 3.5\%$, and sensitivity of 15.21 μV
116 $\text{W}^{-1} \text{m}^{-2}$, while the pyrgeometers operated with a spectral response of 4.5–45 μm , operational
117 errors of $\pm 5.6\%$, and a sensitivity of 12.52 $\mu\text{V} \text{W}^{-1} \text{m}^{-2}$ respectively; typical impedances were ~ 7
118 ohms. All AWS relative humidity values reported here are expressed in terms of saturation vapor
119 pressure over ice.

120 Also during the 2012-13 season, we calibrated and installed five PRD (platinum
121 resistance detector) strings in the upper 5 m of firn in a 2 km survey line extending approximately
122 upwind (grid-west, true-north) starting ~ 50 meters from the on-site AWS. The strings were
123 designed by one of us (AM) following the procedures in Muto et al. [2011]. Each sensor string
124 was 5 m long and consisted of 16 individual PRDs (HEL-700 series; $\pm 0.03^\circ\text{C}$ accuracy, $\pm 0.18^\circ\text{C}$
125 total combined error, including data-logger error) with denser sampling in the shallower firn to



126 capture the greater variability there. Sensor calibration took place over a 60-minute period using a
127 constantly-stirred ice-bath method, and then the newly calibrated sensors were deployed
128 incrementally over a 10-day period starting Dec. 15th. Deployment boreholes were drilled using a
129 4 cm diameter hand-auger, and then back-filled once strings were installed. Campbell logging
130 equipment (CR1000 data logger and AM/16/32 Multiplexer) and 12V sealed lead-acid batteries
131 were housed in a foam-insulated wooden box beside each borehole and just below the surface.
132 The first string was placed 50 m from the AWS, and the other strings were placed upwind of it by
133 10, 100, 1000, and 2000 m (Supplemental Table S2). Measurements were taken every minute
134 over the survey interval. Each 12V battery was swapped out weekly with newly charged
135 replacements to ensure that the sensor strings were continually recording. During each site visit,
136 we took photographs, and noted local meteorological and surface conditions. Each sensor string
137 took approximately 24 hours to equilibrate with the surrounding snow following installation due
138 to the backfilling of the open boreholes with surface snow.

139 We studied crusts in the ice core as well as in the near-surface. As described in
140 Fitzpatrick et al. [2014], the entire deep core and various associated shallower cores were
141 inspected visually during core processing lines at the US National Ice Core Laboratory, primarily
142 by one of us (MS), but with some intercomparisons from other observers. The core was observed
143 on a light table in a darkened booth, and key features were noted on meter-length log books. The
144 crusts were easily visible as thin, glassy, bubble-free or nearly bubble-free layers (e.g. Fig. 1).

145 Annual cycles are visible in the bubbly part of the core, arising from the tendency for
146 near-surface processes to generate coarse-grained, low-density layers including depth hoar in
147 summer [Fitzpatrick et al., 2014; Fegyveresi, 2015]. However, annual-layer dating of the ice core
148 using electrical conductivity (ECM, which is primarily controlled by ice chemistry) and soluble-
149 ion chemistry proved more accurate than dating with visible strata [Buizert et al., 2015; Sigl et al.,
150 2016; WAIS Divide Project Members, 2013]. Here, we estimate the season in which each crust



151 occurs by assigning each summertime peak in the WD2014 time scale to January 1 of its year, and
152 then linearly interpolating; accumulation at the site is relatively evenly distributed through the
153 year, justifying this approximation [Banta et al., 2008; Fegyveresi, 2015, Fegyveresi et al., 2016].

154

155 **3: Observations**

156 **3-1: Near-surface observations**

157 We summarize key observations on crust formation here. Additional information, and
158 complete narrative descriptions of particular crust-forming episodes, are provided in Fegyveresi
159 [2015].

160 Glazed crusts were repeatedly observed to form on the snow surface (Figs. 3 and 4),
161 primarily during late-December and January, with an interval between formation events of
162 roughly one and two weeks (see Figs. 5-8). Crust formation often followed a storm or wind event,
163 and occurred during a time of higher atmospheric pressure, light winds, clear sky, strong
164 insolation, large diurnal temperature cycling, and low relative humidity.

165 As shown in Figure 9, the crusts were often internally complex. The upper few
166 millimeters of firm were anomalously high-density and fine-grained, and might be termed a multi-
167 grain crust. Within this, and especially at the top, were one or more lower-porosity single-grain
168 crusts. To an observer, light reflected off these crusts gave the appearance of a glaze on the snow
169 surface. (e.g. Fig. 4), [see also Orsi et al., 2015, their Fig. 5].

170 Typically, a glazed crust started as isolated sub-meter to few-meter patches on unshaded
171 regions of the snow surface or sastrugi, which were most consistently exposed to sunlight, and
172 spaced tens of meters to more than 100 m apart. Over the first days of formation, glazed crusts
173 expanded to form a laterally extensive interconnected surface broken by isolated sub-meter to
174 few-meter unglazed patches on shaded faces of sastrugi. Glazed crusts were most continuous



175 where the surface was smoothest. Reconnaissance surveys extending a few kilometers from camp
176 showed that glazed-crust formation was consistent at least that far.

177 Within 2-3 days of formation, glazed features developed prominent polygonal cracks
178 with few-meter spacing (e.g. Fig. 4). It is likely that these cracks formed by thermal contraction
179 during nighttime cooling, which was driven by the large diurnal temperature swings observed at
180 the time (see below). We excavated some cracks, which could be traced downward from the
181 surface typically ~20-30 cm.

182 A pronounced hoar began forming within 24 hours of the onset of cracking of the glazed
183 crust in each case observed (e.g. Fig. 3). Measured relative humidity was notably higher during
184 hoar formation (see Figs. 5-8) than before, and sometimes (e.g., January 7th, 2010) a fog
185 developed early in the time of hoar formation, providing a source of vapor to the surface hoar
186 from above. Surface glazing was not required for formation of such hoar layers, as one formed
187 quickly on December 30th, 2009 during a very warm (> -10°) fog episode with elevated measured
188 relative humidity, but without prior formation of surface glaze.

189 Hoar layers that we observed during the field seasons were subsequently either buried,
190 destroyed by wind, or gradually sublimated away over 2-3 additional days. We observed strong
191 winds remove hoar layers, with a threshold of ~7 m s⁻¹ (~13 knots). In one case, crust removal
192 required somewhat lower speed when wind was directed orthogonal to the prevailing direction
193 and thus sastrugi orientation, similar to observations by Champollion et al. [2013] at Dome C,
194 East Antarctica.

195 No above-freezing temperatures were observed by the AWS, but on January 2, 2011, the
196 temperature reached a high of -2.8°C (see Fig. 6; Supplemental Fig. S1). While no direct surface
197 melt was observed, some melt was noted along exposed, vertically cut wall faces near the ice-
198 core drilling facility (Supplemental Fig. S2). A prominent multi-grain crust was observed the next



199 year in snow pits, likely dates from that time, and shows features that are consistent with some
200 melting-refreezing having occurred (Supplemental Fig. S3).

201 The PRD strings document strong variations in subsurface temperature, following the air
202 temperatures as expected. During the cooling phases of diurnal cycles, air temperatures and near-
203 surface firn temperatures dropped well below temperatures deeper in the firn including the
204 shallowest in-firn sensor at ~20 cm (Figs. 10 and 11), with the surface as much as 3°C colder than
205 firn at 40 cm depth (e.g. Supplemental Fig. S4). This would have driven upward mass flux from
206 the firn towards the surface. Such conditions often developed when surface hoar was forming
207 from fog, and thus likely with a downward as well as an upward vapor source to the near-surface
208 layer.

209

210 **3-2: Snow-pit observations**

211 Maps of the shallow pits are presented in Fegyveresi [2015], and an additional paper
212 detailing the isotopic, density, and other data is planned. Relevant here, the pits showed a clear
213 annual cycle in the visual stratigraphy, but with notable “noise”. Depth hoars occurred primarily
214 in summertime layers and into autumn, but with occasional hoar layers in winter and spring
215 layers. Similarly, crusts were most common in summertime and into autumn, but not restricted to
216 those times.

217 Most commonly, crusts occurred just above depth hoars, but crusts were observed
218 without hoar, and hoar without crust. Both single-grain-thick (~1 mm) and multi-grain (≥ 4 mm)
219 crusts were observed, with the common association of single-grain crusts in and usually at the top
220 of multi-grain crusts as noted above. Counting a multi-grain crust containing a single-grain crust
221 as one feature, the 2-meter snow pits revealed an average of $\sim 18.8 \pm 2.5$ ($\pm 1\sigma$) total crusts, or
222 approximately 5 crusts per year.



223 **3-3: Ice-core data**

224 In the bubbly ice included in our crust logging (120-577 m depth) in the WAIS Divide
225 core, 10,268 crusts were identified (Fig. 12). A few were discontinuous across the core, or
226 displayed at least a few pores extending through; others appeared largely or completely
227 continuous and impermeable at the scale of the core. Experience with independent observers
228 showed little or no error in crust identification. We cannot rule out the possibility that bubble
229 migration contributed to loss of some crusts in the deepest bubbly ice considered, but the crusts
230 continued to be clear and readily identifiable, so we do not believe that the trend to fewer crusts
231 in the deepest ice is an artifact. We cannot fully exclude the possibility that there is an
232 observational bias related to the drop in crust prevalence over the most recent ~250 years, as the
233 crusts are more difficult to discern in the shallow firn.

234 The seasonal distribution of the crusts is shown in Figure 13. Crusts occur year-round,
235 but are ~45% more frequent in summertime accumulation than in wintertime. Certainly, the
236 natural variability in seasonal distribution of snow accumulation and in the timing of peak
237 impurity input mean that details of the shape of the seasonal distribution of crust occurrence are
238 notably uncertain. However, given the high reliability of the annual-layer dating, and the multiple
239 indicators that agree well [Buizert et al., 2015; Sigl et al., 2016; WAIS Divide Project Members,
240 2013], “summer” versus “winter” or “nonsummer” should be quite accurate.

241 Time-trends of seasonal crust occurrence are also shown in Supplemental Figure S5,
242 separating the largely sunless winter (May-August) from the sunny spring-summer-fall
243 (September-April, with at least 8 hours of sunlight per day). Both first increase and then decrease
244 slightly over the 2400-year record, but with a larger relative change in the sunlight season.

245
246



247 **4: Discussion**

248 Our observations confirm and extend prior work on this topic. Depositional processes and
249 diagenesis primarily in the upper few centimeters of the firn produce prominent layering.
250 Wintertime accumulation, while notably variable, is more homogeneous than summertime
251 deposits, with wind-packed layers prominent in winter, and more-variable layers including crusts
252 and hoar more common in summer [e.g., Sorge, 1935; Benson, 1962, Gow, 1965; 1969; Weller,
253 1969; Colbeck, 1982; Colbeck, 1983; Alley, 1988; Alley et al., 1997]. These features are altered
254 during subsequent burial and conversion to bubbly ice, but still produce recognizable features in
255 the ice core that allow identification of annual layers and crusts [e.g., Alley et al., 1997;
256 Fitzpatrick et al., 2014].

257 Our observations at WAIS Divide show repeating events that generate the main features
258 of the summertime accumulation. In a typical event, a storm with strong winds brings snow
259 accumulation, followed by a high-pressure system bringing clear skies, greatly reduced winds,
260 initially low humidity, and strong diurnal variations in sunshine, air temperature, and net surface
261 energy-balance.

262 Early in this clear-sky interval, the wind-packed upper surface develops a millimeter-
263 thick glazed crust or possibly crusts in a few-millimeters-thick multi-grain crust. Strengthening of
264 crusts over one to a few days is followed by polygonal cracking from contraction caused by
265 nighttime cooling. Vapor released through the cracks contributes to rising relative humidity, and
266 surface-hoar deposition in subsequent nights. At WAIS Divide, evolution of the crust-hoar
267 complex typically is truncated by arrival of another storm, which may remove or bury the hoar,
268 and typically buries the crusts below the level of fastest diagenesis, allowing them to be
269 preserved.

270 Not every aspect of a typical event is observed in each case. Crusts form and can be
271 buried by additional snowfall without growth of a surface hoar on top of them. Crusts are



272 somewhat discontinuous, and surface hoar can grow where a crust is absent. And, perhaps most
273 importantly here, a crust that remains near the surface (in the upper few centimeters) for too long
274 may slowly lose mass and cease to be a crust.

275 Our data provide strong constraints on models of many of the observed processes.
276 Surface hoar grew especially at night when relative humidity was high, sometimes with fog, and
277 with deposition occurring on tent ropes or other surfaces as well as on the snow surface (e.g.
278 Supplemental Fig. S6), clearly demonstrating a source of vapor from above. Surface hoar
279 typically formed when the upper snow surface was colder than layers beneath, indicating a vapor
280 source from below as well. Hence, our surface hoars included elements of both depositional and
281 sublimation hoar crystals as defined by Gallet et al. [2014] based on observations at Dome C,
282 East Antarctica.

283 The high density of both single-grain and multi-grain crusts, approaching the density of
284 ice for the glassy single-grained crusts, requires that the density of the crusts was increased over
285 time, as wind packing has not been observed to approach these high densities. Crusts form during
286 days when atmospheric humidity is low, however, and thus when mass is not being added from
287 above. We have not observed bulk melting at the site (with the one possible exception noted
288 above), nor do the gas measurements of Orsi et al. [2015] indicate bulk melting, so the density
289 increase must arise from some combination of vapor diffusion from below and surface or volume
290 mass transfer likely involving pseudo-liquid layers [Dash et al., 2006], as discussed next.

291 The data here show that frequently the upper surface is colder than snow beneath, which
292 will lead to upward mass flux. We lack subcentimetric resolution in thermometry, but physical
293 understanding indicates that very strong gradients likely develop on the centimeter scale just
294 below the upper surface during rapid nighttime cooling. Physical understanding, the data here,
295 and data from previously published studies indicate that intense sunshine generates a temperature
296 maximum in the snow just below the surface (order of 1 cm) especially in low-density, low-



297 thermal-conductivity depth hoar [e.g., Alley et al., 1990; Brandt and Warren, 1993], also
298 contributing to upward vapor transport. Hence, the upper surface is expected to gain mass from
299 below during the crust- and hoar-forming events [Alley et al., 1990]. Windy conditions would
300 drive undersaturated air into and out of pore spaces, removing mass, but crusts form during
301 relatively still times. The temperature gradients measured here at WAIS Divide are similar to
302 those observed at GISP2 by Alley et al. [1990] and more than sufficient to move the necessary
303 vapor for crust development.

304 We hypothesize here that these surface conditions cause mass fluxes that fill in open
305 pores in wind-packed layers at the surface to form glazed crusts. A physical model might be
306 based on the following considerations. The thermal conductivity of ice greatly exceeds that of air,
307 so heat transport in firn is primarily conductive. Ordinarily, the grain curvature adjacent to pores
308 tends to cause diffusive mass loss, enlarging pores by filling necks between grains or other
309 regions of lower vapor pressure. However, because heat flow is primarily through the grain
310 structure, pores in a surface crust will tend to be colder than interconnected grains when the upper
311 surface is colder than the firn beneath, favoring mass transport to the pore surfaces, as shown in
312 Figure 14 [e.g., Sommerfeld, 1983; Fukuzawa and Akitaya, 1993]. Transport may occur by vapor,
313 surface, or volume diffusion; following Alley and Fitzpatrick [1999], vapor diffusion and surface
314 transport in premelted films are likely to dominate. Also, mass loss from relatively warm grain
315 bonds just beneath a growing surface crust by diffusion to the colder crust will tend to lower the
316 crust, increasing the likelihood that a pore in the crust will move downward to intersect a pre-
317 existing grain beneath, increasing the crust density.

318 Although summertime crusts dominate in the ice core, many wintertime crusts were
319 identified, raising additional questions. We lack direct observations in winter, and so can only
320 speculate on mechanisms active then. However, the basic picture drawn above for summertime
321 crusts may also apply in winter. The lower temperatures, and lack of intense solar heating, make



322 crust formation less likely. However, stronger wintertime winds would allow greater wind-
323 packing of the upper surface, producing fewer and smaller pores to be filled to make a thin crust,
324 and thus making crust formation easier. Although accumulation is more-or-less evenly distributed
325 through the year, we speculate (based upon variability observed in AWS data) that there may be
326 extended intervals up to weeks in length during the winter when the surface is relatively stable,
327 partially or completely offsetting the slower mass transport from colder temperatures.
328 Furthermore, the AWS data show that mid-winter temperatures have risen as high as -15°C
329 during strong warming events accompanied by high winds ($> 10 \text{ m s}^{-1}$), and likely linked to
330 transport of air masses from the coast. Such warm and windy air masses would produce relatively
331 high vapor pressures, contribute to greater surface packing, and promote temperature inversions
332 and upward near-surface vapor flux during the subsequent cooling.

333 The great abundance of crusts at WAIS Divide compared to other ice cores we have
334 studied may be because conditions are “just right” at WAIS Divide. We have observed loss of a
335 wind-packed crust at WAIS Divide, and also at GISP2 in central Greenland; the strong mass loss
336 from $\sim 1 \text{ cm}$ down in the snowpack is not conducive to long-term survival of any crust there [e.g.,
337 Alley et al., 1990]. Low but nonzero summertime accumulation thus may lead to loss of crusts,
338 whereas higher accumulation after formation buries them below that zone of mass loss and so
339 allows their preservation. The large wintertime variability and high wintertime temperatures at
340 WAIS Divide may be important in generating sufficiently high mass fluxes to produce wintertime
341 crusts.

342 At least in summertime, crusts do seem to record a particular meteorological pattern of
343 storms alternating with still conditions. The time-series of frequency of occurrence of crusts thus
344 would be affected by a change in the frequency of occurrence of these conditions. Turning this
345 into a paleoclimatic indicator would require additional steps, however, as the frequency of
346 preserved crusts could decrease because fewer were formed or because more were destroyed,



347 with different causes. Information on changing frequency of meteorological events might be
348 useful [e.g., Hammer, 1985; Alley, 1988]. We believe that the clear association of crust formation
349 with particular events, and the clear trends in crust occurrence in the core, motivate additional
350 research on topics including crust formation in non-summer seasons, but we do not know whether
351 this ultimately could yield a valuable paleoclimatic indicator.

352 **5: Conclusions**

353 Summertime observations at the WAIS Divide site show that prominent visible strata
354 form at or very near the surface during summer, by processes that typically are repeated a few
355 times during each summer. A storm produces a wind-packed layer. The following high-pressure
356 system brings light winds, warm days and cool nights, strong sunshine, and low relative
357 humidity. High-density, single-grain-thick glazed crusts preferentially form at the surface during
358 these high-pressure intervals, in as little as a single day, and then strengthen and evolve. Crusts
359 are extensive, although typically broken by sub-meter or few-meter uncrusted regions spaced tens
360 of meters to more than 100 m apart. Daytime solar heating drives upward mass transport to crusts
361 from developing depth hoar beneath, strengthening the crusts. After formation, crusts are broken
362 by polygonal cracks extending typically 20-30 cm deep, likely from contraction during nighttime
363 cooling. Relative humidity then rises in the air above, contributing to growth of surface hoar
364 during nighttime cooling. Subsequent storms typically bury the crust-hoar complexes, although
365 crusts can be lost diagenetically during evolving surface conditions if not buried below the top
366 one to a few centimeters.

367 Study of the WAIS Divide deep core shows that crusts are preserved through the bubbly
368 ice. Crusts are most common in layers deposited during summertime, but also occur in winter
369 accumulation. Study of AWS data suggests that the intrusion of warm coastal air during winter



370 may generate strong temperature gradients, which may contribute to wintertime crust formation
371 in wind-packed layers.

372 The frequency of occurrence of crusts in the core varies with time, suggesting the
373 possibility that crusts could be used as a paleoclimatic indicator. However, additional work
374 would be required, including addressing whether crust frequency varies because of changes in
375 formation or changes in destruction of crusts previously formed. The crusts do not produce
376 significant anomalies in other ice-core paleoclimatic records, likely at least in part because they
377 are discontinuous and broken by contraction cracks.

378 **6: Data Availability:**

379 Data policy: All data presented here are available via download from NSIDC
380 (<http://nsidc.org>) or from the WAIS Divide data portal (<http://waisdivide.unh.edu>).
381

382 **7: Author Contribution:**

383 A.J. Orsi assisted with field observations and experiments. A. Muto designed the near-
384 surface PRD sensor strings and developed the associated logging code. M. Spencer documented
385 all ice-core crust observations during the WAIS Divide core processing at the National Ice Core
386 Laboratory. J.M. Fegyveresi and R.B. Alley prepared the manuscript with contributions from all
387 co-authors.
388



389 **8: Acknowledgements:**

390 We acknowledge the following funding sources for support of this work: U.S. National
391 Science Foundation Division of Polar Programs grants 0539578, 1043528, 1142085, 1619793.
392 We also acknowledge Donald E. Voigt, Joan J. Fitzpatrick, Eric D. Cravens, and the staff of the
393 U.S. National Ice Core Laboratory in Denver, Colorado, as well as the WAIS Divide Science
394 Coordination Office at the University of New Hampshire, and the Ice Drilling Design and
395 Operations group at the University of Wisconsin. We thank numerous colleagues involved with
396 the WAIS Divide project, especially Kendrick Taylor, Mark Twickler, and Joseph Souney. We
397 thank Bess Koffman, Gifford Wong, Dominic Winski, Aron Buffen, and Logan Mitchell for
398 assistance with snow pit preparation. Lastly we thank Jonathan Thom and the University of
399 Wisconsin-Madison Automatic Weather Station Program for assistance with weather station
400 sensor installation. Any use of trade, firm, or product names is for descriptive purposes only and
401 does not imply endorsement.

402

403

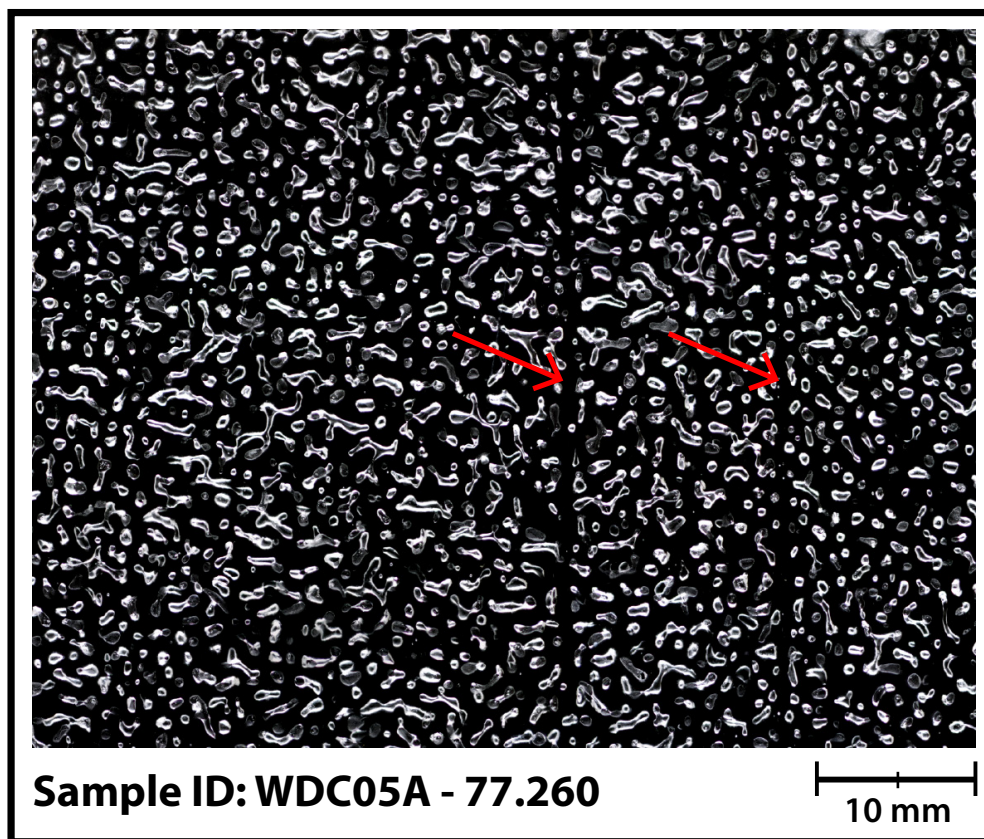


404 9: References

- 405 Alley, R.B., 1988. Concerning the deposition and diagenesis of strata in polar firn. *Journal of*
406 *Glaciology*, 34: 283-290.
- 407 Alley, R.B., Saltzman, E.S., Cuffey, K.M. and Fitzpatrick, J.J., 1990. Summertime formation of
408 depth hoar in central Greenland. *Geophysical Research Letters*, 17(13): 2393-2396,
409 doi:[10.1029/GL017i013p02393](https://doi.org/10.1029/GL017i013p02393).
- 410 Alley, R.B. and Fitzpatrick, J.J., 1999. Conditions for bubble elongation in cold ice-sheet ice.
411 *Journal of Glaciology*, 45(149): 147-153.
- 412 Alley, R.B., Shuman, C.A., Meese, D.A., Gow, A.J., Taylor, K.C., Cuffey, K.M., Fitzpatrick, J.J.,
413 Grootes, P.M., Zielinski, G.A., Ram, M. and Spinelli, G., 1997. Visual-stratigraphic
414 dating of the GISP2 ice core: Basis, reproducibility, and application. *Journal of*
415 *Geophysical Research: Oceans*, 102(C12): 26367-26381, doi:[10.1029/96JC03837](https://doi.org/10.1029/96JC03837).
- 416 Banta, J.R., McConnell, J.R., Frey, M.M., Bales, R.C. and Taylor, K., 2008. Spatial and temporal
417 variability in snow accumulation at the West Antarctic Ice Sheet Divide over recent
418 centuries. *Journal of Geophysical Research: Atmospheres*, 113(D23), doi:
419 [10.1029/2008JD010235](https://doi.org/10.1029/2008JD010235).
- 420 Battle, M.O., Severinghaus, J.P., Sofen, E.D., Plotkin, D., Orsi, A.J., Aydin, M., Montzka, S.A.,
421 Sowers, T. and Tans, P.P., 2011. Controls on the movement and composition of firn air at
422 the West Antarctic Ice Sheet Divide. *Atmospheric Chemistry and Physics*, 11(21), 11007-
423 11021, doi:[10.5194/acp-11-11007-2011](https://doi.org/10.5194/acp-11-11007-2011).
- 424 Benson, C.S., 1962. Stratigraphic Studies on Greenland Ice Sheet and a Quantitative
425 Classification of Glaciers. *Bulletin of the American Meteorological Society*, 43(4): 141.
- 426 Brandt, R.E. and Warren, S.G., 1993. Solar-heating rates and temperature profiles in Antarctic
427 snow and ice. *Journal of Glaciology*, 39(131), 99-110.
- 428 Buizert, C. et al., 2015. The WAIS Divide deep ice core WD2014 chronology–Part 1: Methane
429 synchronization (68–31 ka BP) and the gas age–ice age difference. *Climate of the Past*,
430 11(2): 153-173, doi:[10.5194/cp-11-153-2015](https://doi.org/10.5194/cp-11-153-2015).
- 431 Champollion, N., Picard, G., Arnaud, L., Lefebvre, E. and Fily, M., 2013. Hoar crystal
432 development and disappearance at Dome C, Antarctica: observation by near-infrared
433 photography and passive microwave satellite. *The Cryosphere*, 7(4): 1247-1262,
434 doi:[10.5194/tc-7-1247-2013](https://doi.org/10.5194/tc-7-1247-2013).
- 435 Colbeck, S.C., 1982. An overview of seasonal snow metamorphism. *Reviews of Geophysics*,
436 20(1): 45-61.
- 437 Colbeck, S.C., 1983. Theory of metamorphism of dry snow. *Journal of Geophysical Research:*
438 *Oceans*, 88(C9): 5475-5482.
- 439 Das, S.B. and Alley, R.B., 2005. Characterization and formation of melt layers in polar snow:
440 observations and experiments from West Antarctica. *Journal of Glaciology*, 51(173):
441 307-312, doi:[10.3189/172756505781829395](https://doi.org/10.3189/172756505781829395).
- 442 Dash, J.G., Rempel A.W., and Wettlaufer J.S., 2006. The physics of premelted ice and its
443 geophysical consequences, *Rev. Mod. Phys.* 78, 695-741,
444 doi:[10.1103/RevModPhys.78.695](https://doi.org/10.1103/RevModPhys.78.695).
- 445 Fegyveresi, J.M., 2015, Physical properties of the West Antarctic Ice Sheet (WAIS) Divide deep
446 core: Development, evolution, and interpretation, PhD thesis, The Pennsylvania State
447 Univ., State College, Pa.
- 448 Fegyveresi, J.M., Alley, R.B., Fitzpatrick, J.J., Cuffey, K.M., McConnell, J.R., Voigt, D.E.,
449 Spencer, M.K. and Stevens, N.T., 2016. Five millennia of surface temperatures and ice
450 core bubble characteristics from the WAIS Divide deep core, West Antarctica.
451 *Paleoceanography*, 31: 416–433, doi:[10.1002/2015PA002851](https://doi.org/10.1002/2015PA002851).

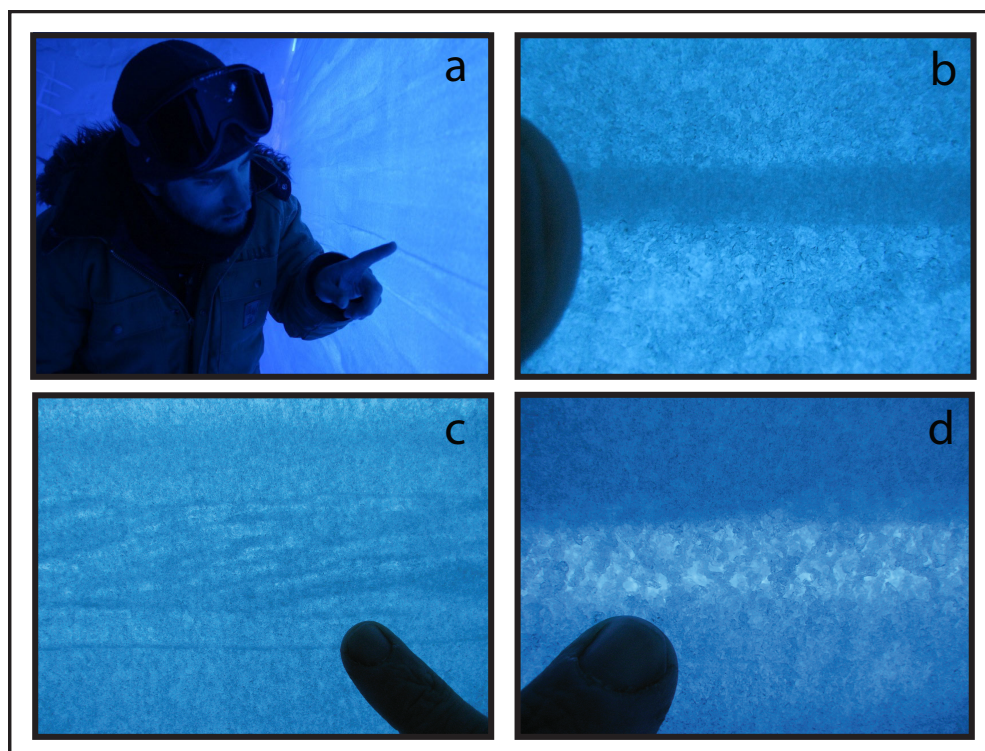


- 452 Fitzpatrick, J.J., Voigt, D.E., Fegyveresi, J.M., Stevens, N.T., Spencer, M.K., Cole-Dai, J., Alley,
453 R.B., Jardine, G.E., Cravens, E.D., Wilen, L.A. and Fudge, T.J., 2014. Physical
454 properties of the WAIS Divide ice core. *Journal of Glaciology*, 60(224), 1181-1198,
455 doi:[10.3189/2014JoG14J100](https://doi.org/10.3189/2014JoG14J100).
- 456 Fukuzawa, T. and Akitaya E., 1993. Depth-Hoar Crystal-Growth in the Surface-Layer under
457 High-Temperature Gradient. *Annals of Glaciology*, 18: 39-45.
- 458 Gallet, J.C., Domine, F., Savarino, J., Dumont, M. and Brun, E., 2014. The growth of sublimation
459 crystals and surface hoar on the Antarctic plateau. *The Cryosphere*, 8(4): 1205-1215,
460 doi:[10.5194/tc-8-1205-2014](https://doi.org/10.5194/tc-8-1205-2014).
- 461 Gow, A. 1965. On the accumulation and seasonal stratification of snow at the South Pole. *Journal*
462 *of Glaciology*, 5(40): 467-477.
- 463 Gow, A. 1969. On the rates of growth of grains and crystals in south polar firn. *Journal of*
464 *Glaciology*, 8(53): 241-252.
- 465 Hammer, C.U., 1985. The influence on atmospheric composition of volcanic eruptions as derived
466 from ice-core analysis. *Annals of Glaciology*, 7: 125-129.
- 467 Koerner, R.M. 1971. A stratigraphic method of determining the snow accumulation at Plateau
468 Station, Antarctica, and application to South Pole-Queen Maud Land traverse 2, 1965-
469 1966. In Crary, A.P. *Antarctic snow and ice studies II*, (Washington, DC, American
470 Geophysical Union): 225-238.
- 471 Lazzara, M.A., Weidner, G.A., Keller, L.M., Thom J.E., and Cassano, J.J., 2012. Antarctic
472 Automatic Weather Station Program 30 Years of Polar Observations. *Bulletin of the*
473 *American Meteorological Society*, 93(10): 1519-1537, doi:[10.1175/BAMS-D-11-00015.1](https://doi.org/10.1175/BAMS-D-11-00015.1).
- 474
475 Mitchell, L.E., Buizert, C., Brook, E.J., Breton, D.J., Fegyveresi, J., Baggenstos, D., Orsi, A.,
476 Severinghaus, J., Alley, R.B., Albert, M. and Rhodes, R.H., 2015. Observing and
477 modeling the influence of layering on bubble trapping in polar firn. *Journal of*
478 *Geophysical Research: Atmospheres*, 120(6): 2558-2574, doi:[10.1002/2014JD022766](https://doi.org/10.1002/2014JD022766).
- 479 Muto, A., Scambos, T.A., Steffen, K., Slater, A.G. and Clow, G.D., 2011. Recent surface
480 temperature trends in the interior of East Antarctica from borehole firn temperature
481 measurements and geophysical inverse methods. *Geophysical Research Letters*, 38(15),
482 doi:[10.1029/2011GL048086](https://doi.org/10.1029/2011GL048086).
- 483 Orsi, A.J., Kawamura, K., Fegyveresi, J.M., Headly, M.A., Alley, R.B. and Severinghaus, J.P.,
484 2015. Differentiating bubble-free layers from melt layers in ice cores using noble gases.
485 *Journal of Glaciology*, 61(227): 585-594, doi:[10.3189/2015JoG14J237](https://doi.org/10.3189/2015JoG14J237).
- 486 Sigl, M. et al., 2016. The WAIS Divide deep ice core WD2014 chronology–Part 2: Annual-layer
487 counting (0–31 ka BP). *Climate of the Past*, 12(3): 769-786, doi:[10.5194/cp-12-769-2016](https://doi.org/10.5194/cp-12-769-2016).
- 488
489 Sommerfeld, R.A., 1983. A branch grain theory of temperature gradient metamorphism in snow.
490 *Journal of Geophysical Research: Oceans*, 88(C2): 1484-1494,
491 doi:[10.1029/JC088iC02p01484](https://doi.org/10.1029/JC088iC02p01484).
- 492 Sorge, E., 1935. Glaziologische Untersuchungen in Eismitte. *Brockamp, B., and others.*
493 *Glaziologie. Leipzig, FA Brockhaus*, 935: 62-270.
- 494 WAIS Divide Project Members, 2013. Onset of deglacial warming in West Antarctica driven by
495 local orbital forcing. *Nature*, 500(7463): 440-444, doi:[10.1038/nature12376](https://doi.org/10.1038/nature12376).
- 496 Weller, G. 1969. The heat and mass balance of snow dunes on the central Antarctic Plateau.
497 *Journal of Glaciology*, 8: 277-284.
- 498
499
500



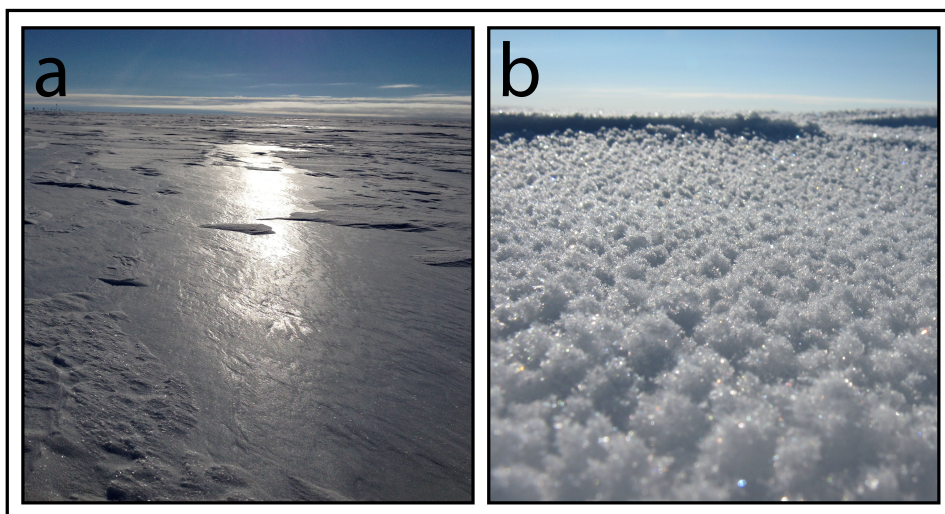
501
502

503 **Figure 1:** A thick-section image of a sample prepared from a depth of ~77.260 meters showing
504 two preserved crusts. Both layers are ~1 mm thick and appear mostly bubble-free. All bubbles
505 here appear white, with the surrounding ice black. The general elongated shape of the bubbles is
506 due the proximity of this sample to the bubble close-off depth at WAIS Divide of ~75 meters).
507 This sample is from the secondary WDC05A core at the WAIS Divide site. Image modified from
508 Orsi et al. [2015].

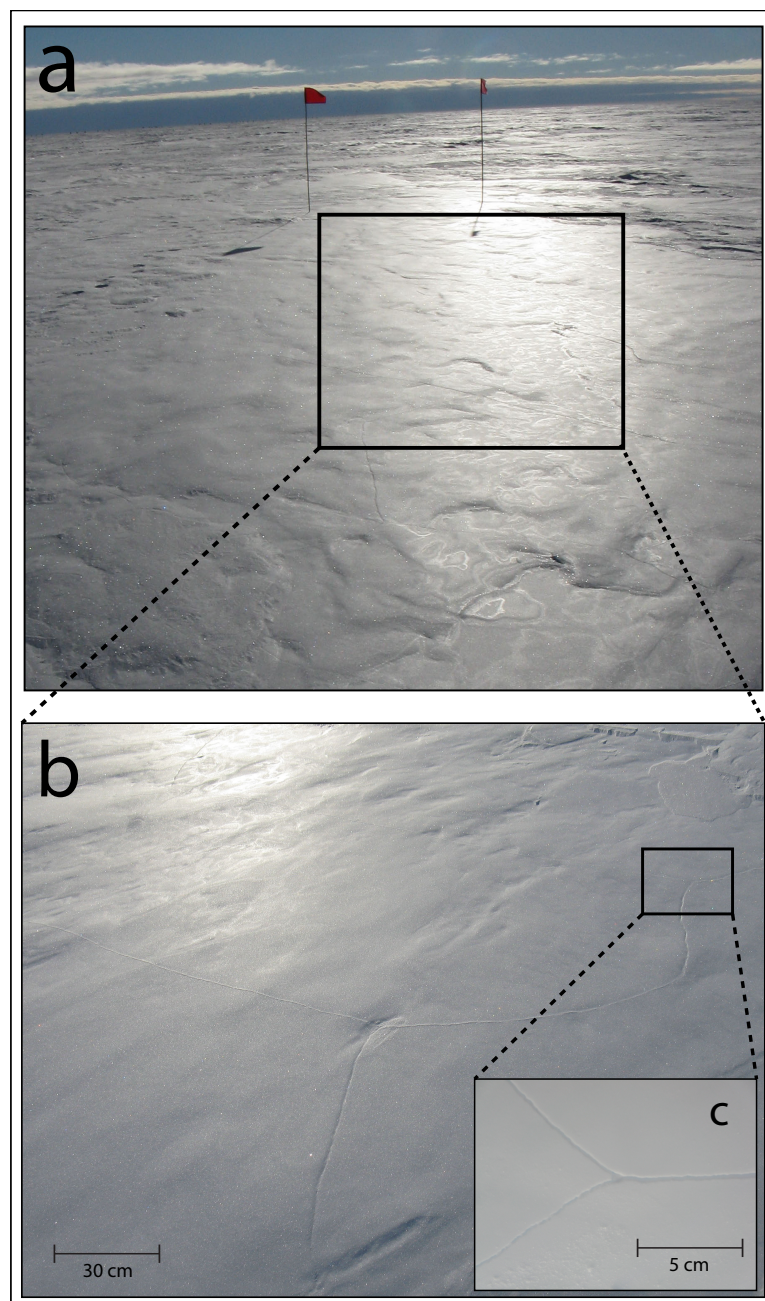


509
510
511
512
513

Figure 2: The lead author in a 2-meter snow pit prepared at WAIS Divide (pit 2009-10-A). Multi-grain crusts (a, b), preserved sastrugi with cross-bedding (c), and hoar layers (d) are all easily identifiable.

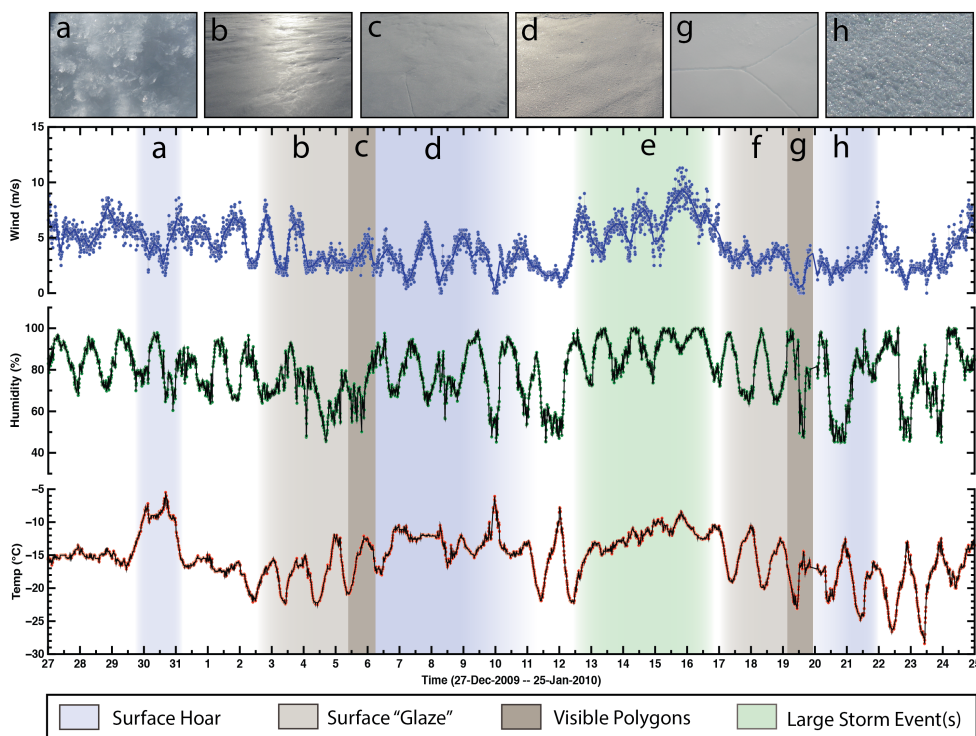


514
515 **Figure 3:** Surface “glaze” (a) that formed on a calm, sunny day (23-Dec-2012) at WAIS Divide,
516 and the subsequent surface hoar layer (b) that formed on its surface after several calm days.



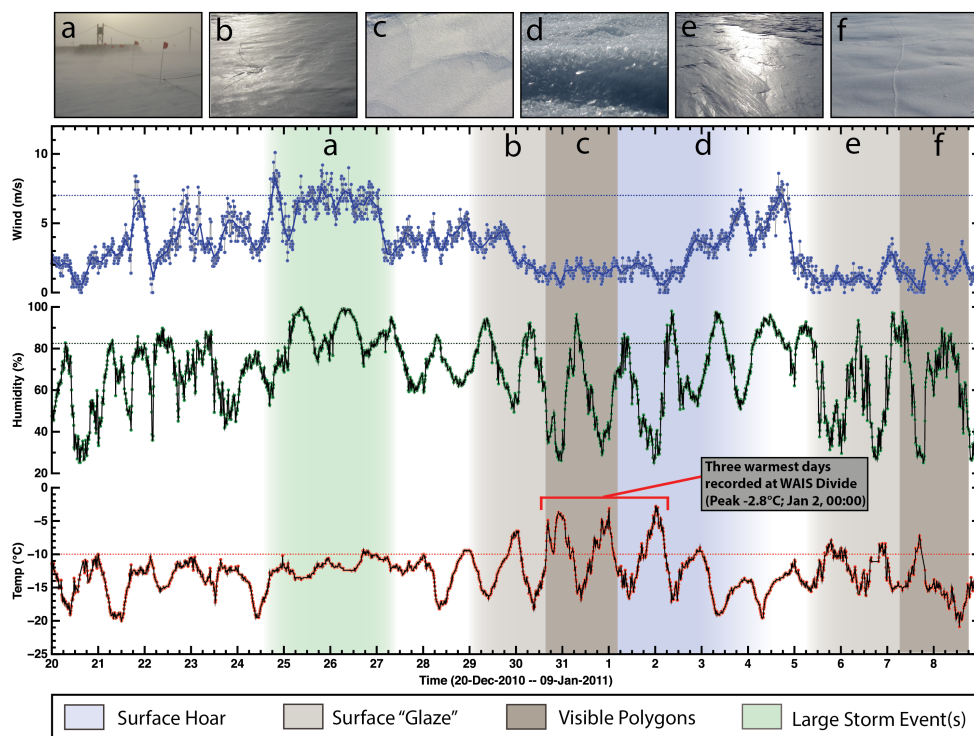
517
518
519
520
521

Figure 4: Surface “glaze” seen at the WAIS Divide site. (a). A zoomed-in view shows the polygonal cracking that initiates at the surface from thermal contraction, following several sunny, clear-sky days (b). Closer inspection reveals greater detail and scale of a crack triple-junction (c).



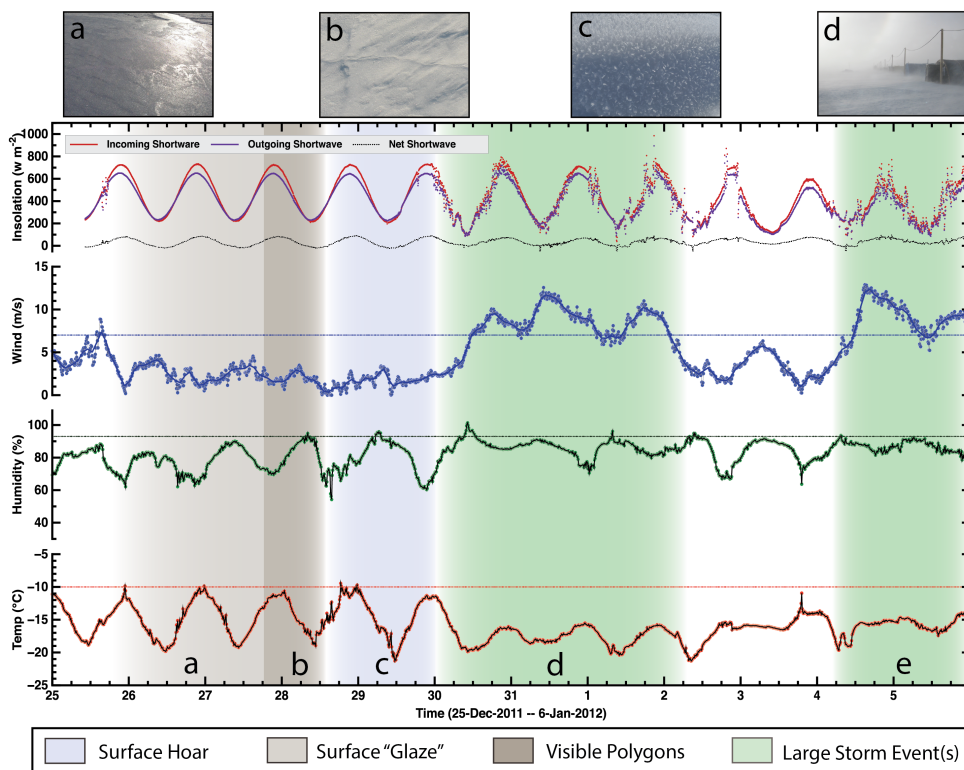
522
523
524
525
526
527
528

Figure 5: Surface evolution over 29 days in 2009-10 season, and AWS data. Shading shows episodes of surface hoar, glazes, and polygonal cracking; storm events are also shown. Letters near the top refer to photographs above of specific features or events. All dates and times are GMT (-12 WAIS local time). The errors for all AWS instruments are listed in Supplemental Table S1.



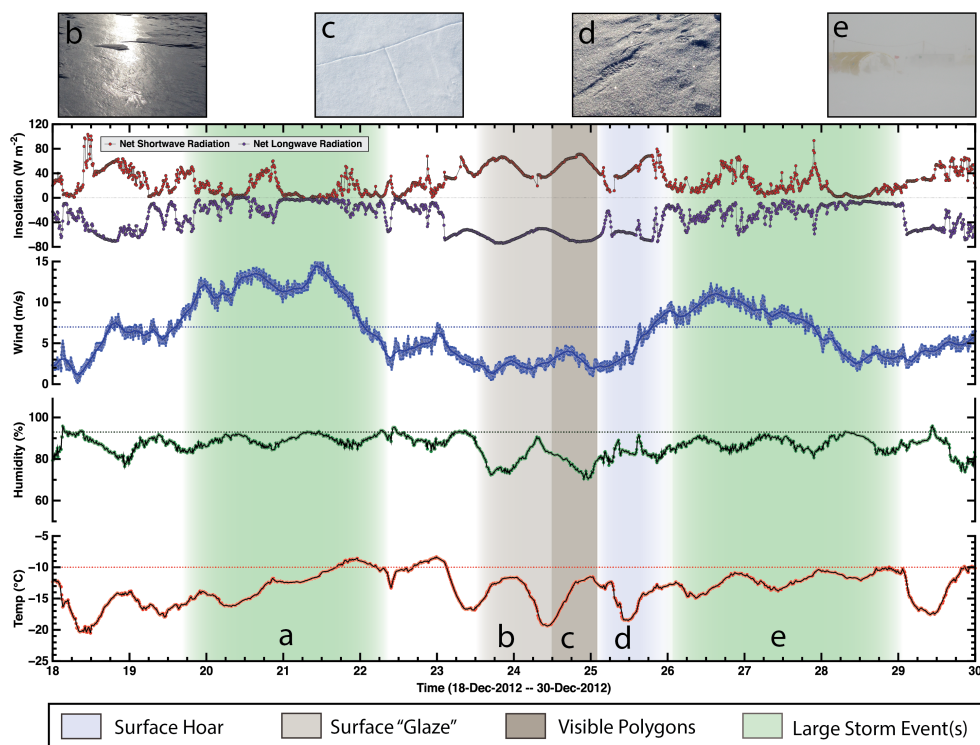
529
530
531
532
533
534
535

Figure 6: Surface evolution over 20 days in 2010-11 season, and AWS data. Shading shows episodes of surface hoar, glazes, and polygonal cracking; storm events are also shown. Letters near the top refer to photographs above of specific features or events. All dates and times are GMT (-12 WAIS local time). The errors for all AWS instruments are listed in Supplemental Table S1.



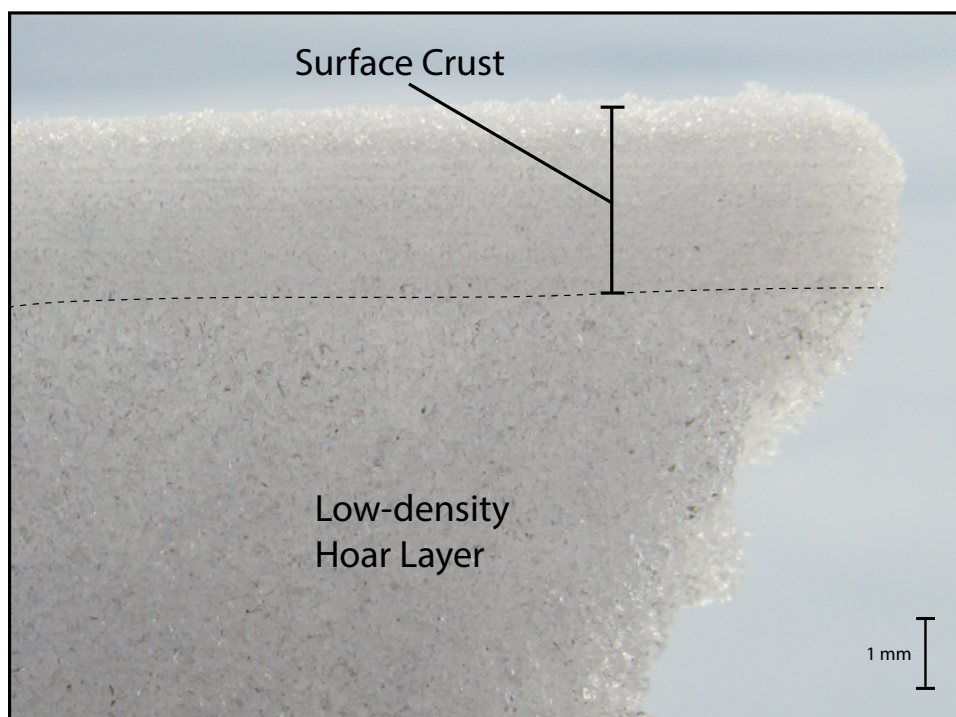
536
 537
 538
 539
 540
 541
 542

Figure 7: Surface evolution over 12 days in 2011-12 season, and AWS data. Shading shows episodes of surface hoar, glazes, and polygonal cracking; storm events are also shown. Letters near the top refer to photographs above of specific features or events. All dates and times are GMT (-12 WAIS local time). The errors for all AWS instruments are listed in Supplemental Table S1.



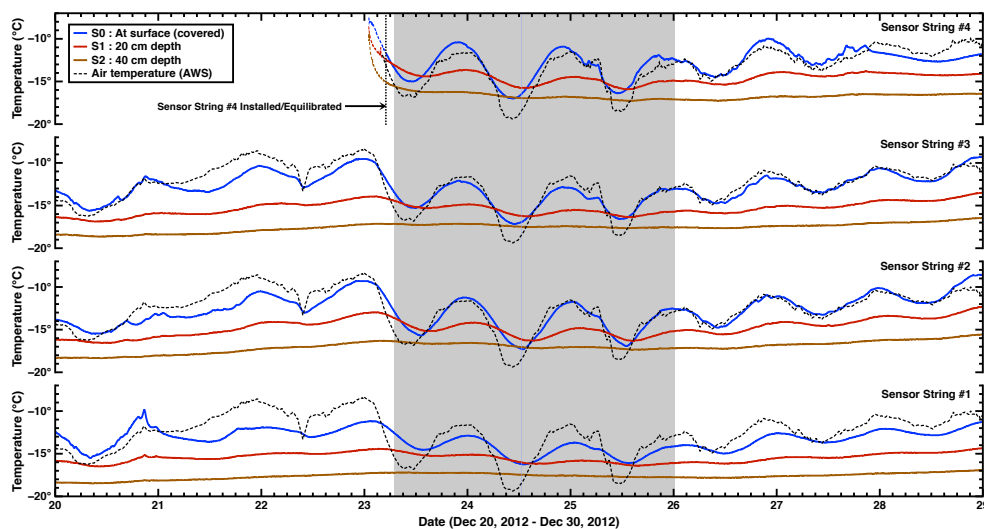
543
544
545
546
547
548
549

Figure 8: Surface evolution over 12 days in 2012-13 season, and AWS data. Shading shows episodes of surface hoar, glazes, and polygonal cracking; storm events are also shown. Letters near the top refer to photographs above of specific features or events. All dates and times are GMT (-12 WAIS local time). The errors for all AWS instruments are listed in Supplemental Table S1.



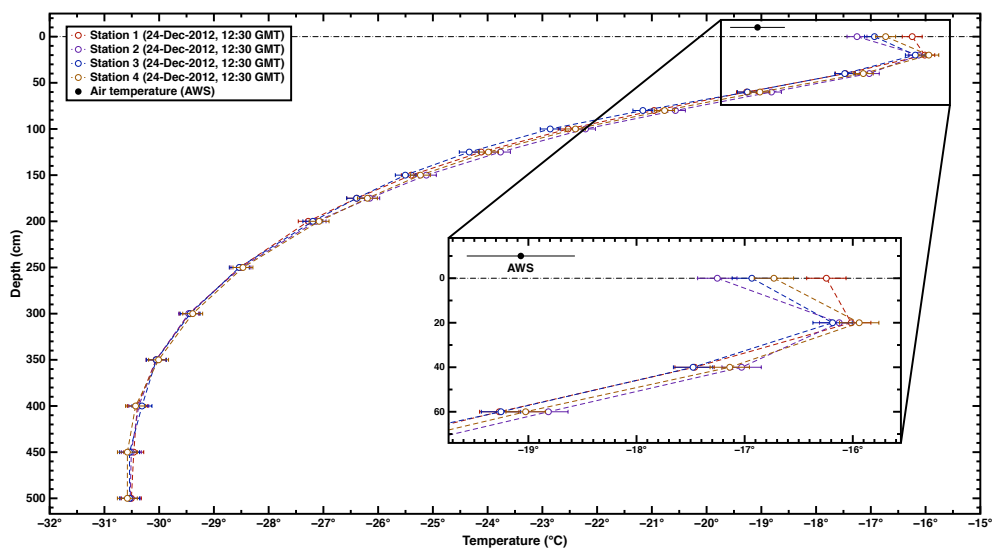
550
551
552
553
554

Figure 9: A firm sample excavated from a glazed area at WAIS Divide before the onset of polygonal cracking, showing a couplet of an evolved high-density ~3 mm multi-grain surface crust containing single-grain crusts, and overlying a lower-density hoar layer.



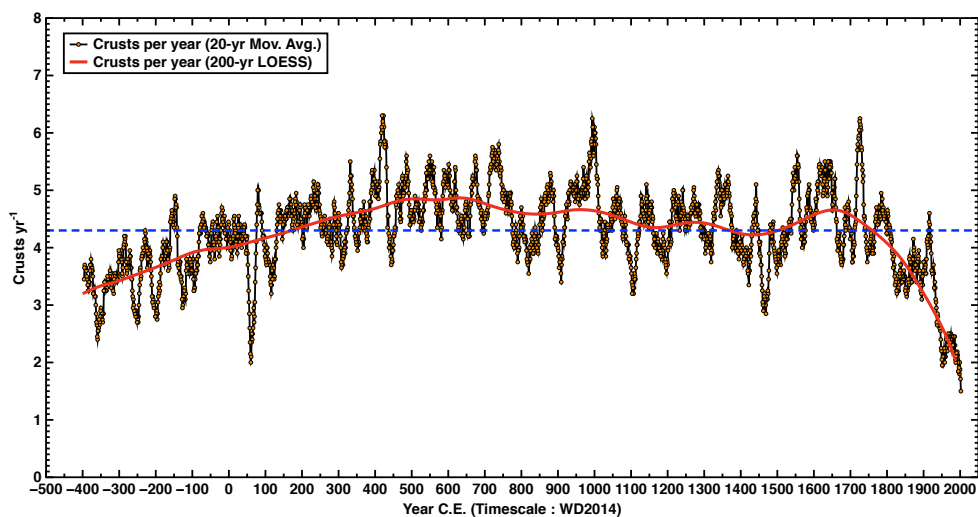
555
556

557 **Figure 10:** Temperature measurements (1 min interval) in firn from the 2012-13 season, from the
558 upper-most three PRDs (surface down to 40 cm). Data are from the four sensor stations closest to
559 the station. The shaded area corresponds to an episode of glaze and hoar growth (see Fig. 8).
560 Distinct near-surface temperature inversions occurred each night during this 3-day period (see
561 Fig. 11). Sensor #4 was not installed until Dec 22nd, and therefore did not equilibrate until early
562 on the 23rd as indicated. Air temperature is also shown as recorded by the AWS (errors listed in
563 Supplemental Table S1). The AWS temperature sensor is located ~1 meter above the snow
564 surface. All dates and times are GMT (-12 WAIS local time).



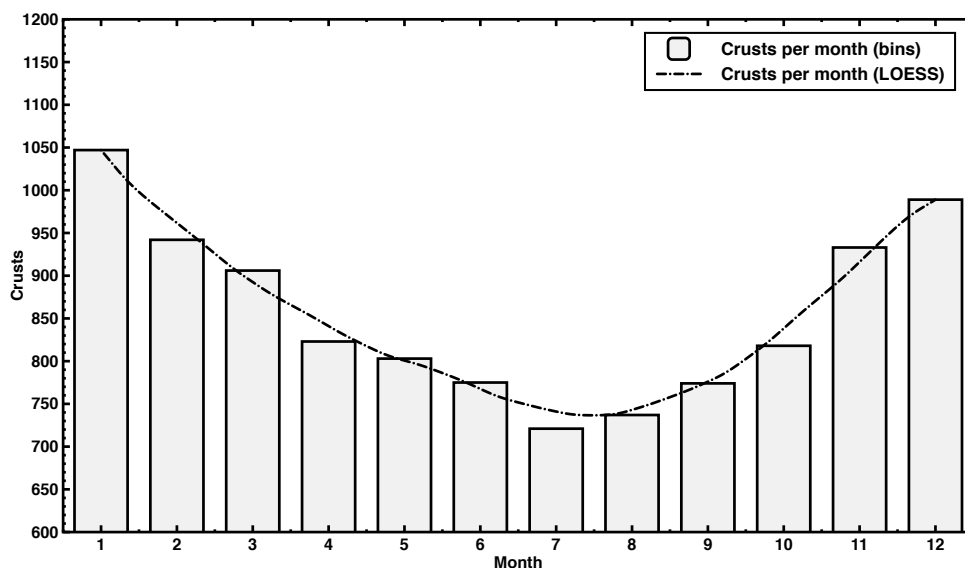
565
566
567
568
569

Figure 11: Snap-shot temperature readings for PRD-string stations #1-4, taken on 24-Dec-2012 at ~12:30 GMT, showing the temperature inversion with colder air (AWS data) and upper surface over warmer near-surface firn.



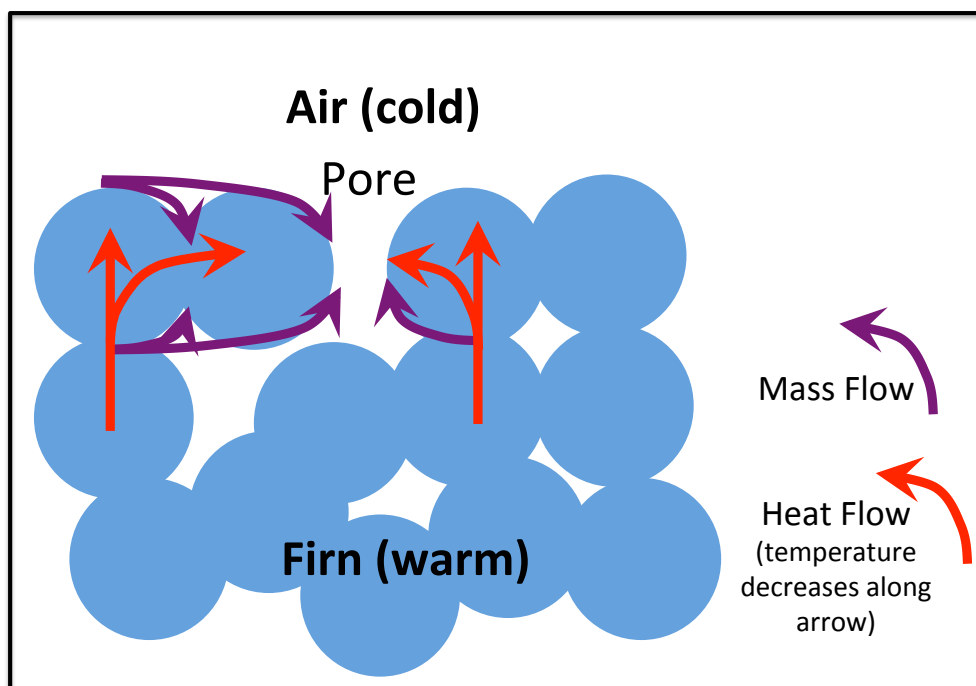
570
571

572 **Figure 12:** History of crust occurrence (crusts year⁻¹) in the bubbly-ice zone of the WDC06A
573 core that we studied in detail (~120 – 577 m depth); ages (C.E.) are from the WD2014 depth-age
574 scale). 10,268 unique crusts were documented in the core, for an average rate of 4.3 ± 2 per year
575 (dashed blue line). Data are shown as 20-yr moving averages for ease of view, with an added 1st-
576 order LOESS smoothing trend-curve (200-yr bin-width). The sharp decline in crust prevalence
577 after ~1750 C.E. may be due to observational biasing in the shallow firn.



578
579

580 **Figure 13:** Crust distribution by month (1=January, 2=February,...12=December) based on
581 assumption that each summer pick in the WD2014 depth-age scale is January 1, and then
582 interpolating linearly. Crusts occur year-round but more commonly in summer accumulation. The
583 smoothed curve is a 1st-order LOESS trend curve (width = 2).



584

585

586 **Figure 14:** Schematic illustrating possible mass and heat transports during formation of a
587 single-grain glazed crust, when the near-subsurface is warmer than the surface. Heat flow is
588 primarily through the grain structure (blue), so pores (white) in the surface layer will be colder
589 than interconnected grains, favoring mass transport from the grains to those pores, increasing
590 density of the surface layer.



591 **Table 1:** Field observation table (see also Figs. 5, 6, 7, 8).

Field Season	Observation Window	Observation Duration	AWS	Other Instrumentation	Pit
2008-2009 ¹	12-Dec-2008 : 10-Jan-2009	~29 days	--	--	x
2009-2010 ¹	27-Dec-2009 : 25-Jan-2010	~29 days	W,H,T	--	x
2010-2011	20-Dec-2010 : 09-Jan-2011	~20 days	W,H,T	--	x
2011-2012 ¹	25-Dec-2011 : 04-Jan-2012	~12 days	W,H,T,I	Dual Li-Cor LI200 sensors Kipp-Zonen CNR2 sensor	x
2012-2013 ¹	18-Dec-2012 : 30-Dec-2012	~12 days	W,H,T,I	Shallow PRD strings ²	x

W,H,T,I - Wind, Humidity, Temperature, Insolation

¹Fegyveresi, 2015

²Muto et al., 2011

592